Article

Double Quantum Ring under an Intense Nonresonant Laser Field: Zeeman and Spin-Orbit Interaction Effects

Miguel E. Mora-Ramos [1], Juan A. Vinasco [2,*], Adrian Radu [3], Ricardo L. Restrepo [4], Alvaro L. Morales [2], Mehmet Sahin [5], Omar Mommadi [6], José Sierra-Ortega [7], Gene Elizabeth Escorcia-Salas [7,8], Christian Heyn [9], Derfrey A. Duque [10] and Carlos A. Duque [2]

[1] Centro de Investigación en Ciencias-IICBA, Universidad Autónoma del Estado de Morelos, Av. Universidad 1001, Cuernavaca CP 62209, Mexico; memora@uaem.mx

[2] Grupo de Materia Condensada-UdeA, Instituto de Física, Facultad de Ciencias Exactas y Naturales, Universidad de Antioquia UdeA, Calle 70 No. 52-21, Medellín 050010, Colombia; alvaro.morales@udea.edu.co (A.L.M.); carlos.duque1@udea.edu.co (C.A.D.)

[3] Department of Physics, "Politehnica" University of Bucharest, 313 Splaiul Independenţei, 060042 Bucharest, Romania; radu@physics.pub.ro

[4] EIA-Física Teórica y Aplicada, Universidad EIA, Envigado 055428, Colombia; ricardo.restrepo@eia.edu.co

[5] Department of Nanotechnology Engineering, Abdullah Gul University, Sumer Campus, 38080 Kayseri, Türkiye; mehmet.sahin@agu.edu.tr

[6] OAPM Group, Laboratory of Materials, Waves, Energy and Environment, Department of Physics, Faculty of Sciences, University Mohamed I, Oujda 60000, Morocco; omommadi@gmail.com

[7] Grupo de Investigación en Teoría de la Materia Condensada, Universidad del Magdalena, Santa Marta 470004, Colombia; jcsierra@unimagdalena.edu.co (J.S.-O.); geneescorcias@unicesar.edu.co (G.E.E.-S.)

[8] Grupo de Óptica e Informática, Departamento de Física, Universidad Popular del Cesar, Sede Hurtado, Valledupar 200001, Colombia

[9] Center for Hybrid Nanostructures (CHyN), University of Hamburg, Luruper Chaussee 149, 22761 Hamburg, Germany; heyn@physnet.uni-hamburg.de

[10] GICEI, Facultad de Ingeniería, Institución Universitaria Pascual Bravo, Medellín 050034, Colombia

* Correspondence: juan.vinascos@udea.edu.co

Abstract: We theoretically investigate the properties of an electron energy spectrum in a double GaAs-Al$_{0.3}$Ga$_{0.7}$As quantum ring by using the effective mass and adiabatic approximations, together with a realistic description of the confining potential profile, which is assumed to be deformed due to the application of an intense nonresonant laser field. The effects of the applied magnetic field and spin-orbit interaction are included. We discuss the features of the lowest confined energy levels under a variation of magnetic field strengths and intense laser parameters. The influence of this external probe on the linear optical absorption response associated with interlevel transitions is analyzed by considering both the presence and absence of spin-orbit effects.

Keywords: double quantum ring; intense laser field; Rashba and Dresselhaus spin-orbit interactions; Zeeman effect

1. Introduction

Due to their unique electronic and optical properties, semiconductor quantum rings (QRs) have shown great promise for various opto-electronic applications. These nanostructures are a potential building block for next-generation opto-electronic devices, offering advantages over traditional quantum dots and other semiconductor nanostructures. QRs can efficiently confine charge carriers, generating single photons by recombining an electron-hole pair. This property makes QRs excellent candidates for single-photon emitters. Studies have demonstrated the feasibility of utilizing QRs as efficient single-photon sources [1–3]. In addition to single-photon emitters, the unique energy levels in QRs can lead to low-threshold lasing, enabling the development of compact and energy-efficient

lasers [4,5]. Furthermore, semiconductor QRs have shown promise for applications in photodetection and photovoltaics. The engineered energy spectrum in QRs can be tailored to match specific wavelengths, making them suitable for wavelength-tunable photodetectors [6,7]. As for photovoltaics, QRs have been studied for their potential to enhance light absorption and charge separation, which could lead to improved efficiency in solar cells [8,9]. Another emerging application of semiconductor QRs is in spintronics. Spin-orbit coupling in QRs can enable efficient manipulation and control of spin states, which is essential for spin-based electronic devices [10,11]. The effects of spin-orbit interaction (SOI) on the opto-electronic properties of QRs have also been investigated [12–15].

When considering a one-dimensional QR, the optically induced Aharonov-Bohm effect in mesoscopic rings has been reported by Sigurdsson and coworkers [16]. They show, theoretically, that strong electron coupling to circularly polarized photons in non-singly connected nanostructures results in an artificial gauge field that changes the electron phase, which is analogous to the well-known Aharonov-Bohm phase effect. Within the Floquet theory of periodically driven quantum systems, Kozin et al. studied the electronic properties of semiconductor quantum rings with the Rashba spin-orbit interaction irradiated by an off-resonant high-frequency electromagnetic field, finding a relevant modification of all the electronic characteristics of the rings under the dressing field effects (see, for instance, [17] and the references therein). The previous study has been extended to a two-dimensional QR array, demonstrating that a strong high-frequency circularly polarized electromagnetic field can turn a two-dimensional periodic array of interconnected QRs into a topological insulator [18].

Double semiconductor quantum rings (DSQRs) generally consist of two concentric rings with different bandgap materials, leading to interesting quantum confinement effects. The confinement in the radial and azimuthal directions gives rise to a rich energy spectrum and various optical transitions. Several research works have delved into the properties and potential applications of DSQRs. For instance, experimental realizations of these particular nanostructures have appeared at different moments. Kuroda and collaborators first reported on the fabrication of concentric DQRs and investigated the excitonic transitions in those structures [19,20]. Transport in Coulomb-coupled double rings under a magnetic field was measured in Ref. [21], whereas Kim reported on the optical transitions in GaAs-Al$_{0.3}$Ga$_{0.7}$As DQRs grown by droplet epitaxy [22].

Theoretically speaking, reports on electronic states in concentric DQRs were published early, for instance, by Li et al., within the framework of the effective mass envelope function approach [23], and by Planelles and Climente, including magnetic field effects [24]. The influence of an applied, intense nonresonant laser field on the electronic and optical properties of semiconductor DSQRs has been dealt in several previous works [25–27], and the systematic treatment on optical absorption in concentric DQRs was recently put forward [28].

Here, we aim to present a theoretical investigation of the electronic properties of double concentric QRs by considering the influence of externally applied nonresonant intense lasers and magnetic fields and the effect of spin-orbit coupling. Knowledge about electron states allows for an evaluation of the system's interlevel linear optical absorption response. The adiabatic approximation is assumed to separate the vertical from the in-plane electron motions for the calculation. The solution for the latter is then tackled by using the finite element method. The article is organized as follows: Section 2 establishes the theoretical model used in this article. Section 3 presents the results, with and without considering SOI, along with the corresponding discussion. Section 4 summarizes the main findings.

2. Theoretical Framework

The system under study is a GaAs double ring embedded in an Al$_{0.3}$Ga$_{0.7}$As matrix under the combined effects of a magnetic field in the *z*-direction and a nonresonant laser

field (ILF). The geometry shown in Figure 1a was generated from the profile data of the AFM measurements from the work of Kuroda et al. [19].

Under the effects considered, the Schrödinger equation for a confined electron can be expressed by

$$H\,\boldsymbol{\psi}(x,y,t) = i\hbar\,I_2\,\frac{\partial}{\partial t}\boldsymbol{\psi}(x,y,t), \tag{1}$$

where $\boldsymbol{\psi} = \begin{pmatrix} \psi_\uparrow \\ \psi_\downarrow \end{pmatrix}$ is the wave function in a vector, with the components representing spin up and spin down. $H = \begin{pmatrix} H_{11} & H_{12} \\ H_{21} & H_{22} \end{pmatrix}$, $\hbar$ is the reduced Planck constant, and I_2 is the 2×2 identity matrix. The Hamiltonian can be written as the sum of several contributions:

$$H \;=\; H_0 I_2 + \frac{1}{2}g\mu B\sigma_z + H_R + H_D \tag{2}$$

where

$$H_0 \;=\; \frac{\hbar^2 k^2}{2\,m_c^*} + V(h(x,y))\,. \tag{3}$$

Here, $h(x,y)$ is the height, and it is a function of the position in the (x,y)-plane. Note that in Equation (3), the confinement potential is a function of the QR's height, which is a function of the coordinates in the (x,y)-plane. In this case, we use the adiabatic approximation to convert a 3D problem into a 2D problem, where the confinement potential in the ring region is given by the energy associated with a quantum well of width h with finite potential barriers (the height of the barrier in the whole space is obtained from the product between the band offset and the gap difference between the well and barrier materials). By using the adiabatic approximation, in this study, we propose that the ring height along the z-axis in all of the space is generally much smaller with respect to the dimensions of the ring in the (x,y)-plane. More details on the method can be viewed in [29]. In other words, the fast movement occurs along the z-direction, whereas the slow movement occurs along the (x,y)-plane.

Since we have cylindrical symmetry, equal radii $\sqrt{x^2+y^2}$ have the same height, $\mathbf{k} = -i\,\nabla + \frac{e}{\hbar}(\mathbf{A}_m + \mathbf{A}_l)$, g is the Landé factor, μ_B is the Bohr magneton, B is magnetic Field, σ_j ($j = x, y, z$) are the j component of the Pauli matrices vector, m_c^* is the effective mass with $c = w, b$ for the GaAs double quantum ring and $Al_{0.3}Ga_{0.7}As$ matrix, respectively. The terms H_R and H_D are the Rashba and Dresselhaus spin-orbit interactions, respectively.

This system is taken to be under external magnetic and nonresonant intense laser field (ILF) effects. The incident ILF was defined for elliptical and linear polarizations. The vector potential of the laser field is given by

$$\mathbf{A}_l(t) = \left(\mathbf{x}\cos(\omega t) + \kappa\,\mathbf{y}\cos\left(\omega t + \frac{\pi}{2}\right)\right)A_0, \tag{4}$$

where $\mathbf{x}$ and $\mathbf{y}$ are the unit vectors, A_0 is the amplitude, ω is the frequency of the laser field, and $\kappa = 0, 1$ is the linear and right circularly polarizations, respectively.

For the applied magnetic field, $\mathbf{B} = B\,\mathbf{z}$. It uses the symmetry gauge $\mathbf{A}_m = \frac{B}{2}(y\,\mathbf{x} - x\,\mathbf{y})$, with $\mathbf{B} = -\nabla \times \mathbf{A}_m$.

When applying the Kramers-Henneberger transformation [30] to Equation (3), it becomes a time-independent Schrödinger equation

$$H'\,\boldsymbol{\phi}(x,y) = E\,I_2\,\boldsymbol{\phi}(x,y), \tag{5}$$

where the H_0 term becomes

$$H_0' \;=\; \frac{\hbar^2 \nabla_{x,y}^2}{2\,m_c^*} + i\frac{e\,B\,\hbar}{2\,m_c^*}(y\,\mathbf{x} - x\,\mathbf{y})\cdot\nabla + V_d(x,y)\,. \tag{6}$$
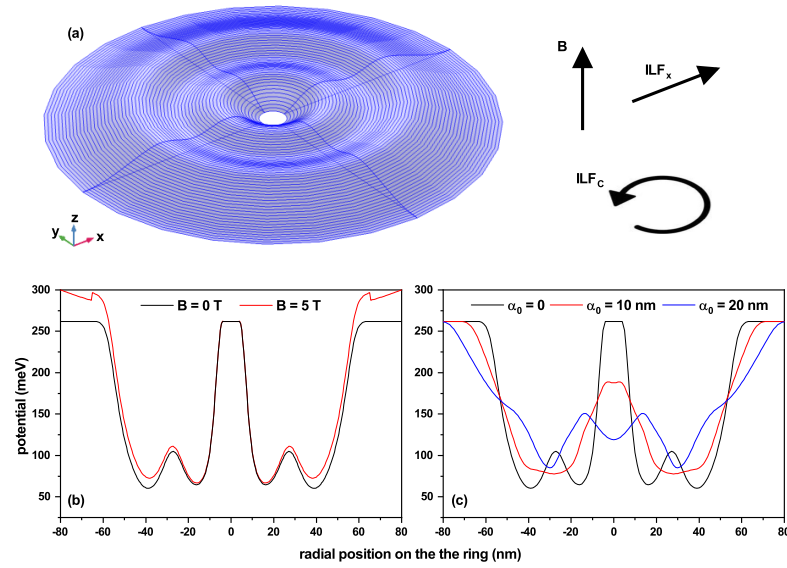
Figure 1. (**a**) Schematic representation of a double GaAs-Al$_{0.3}$Ga$_{0.7}$As quantum ring, with the profile taken from the work of Kuroda et al. [19]. The drawn vectors represent a magnetic field B in the z-direction, a nonresonant intense laser field for x, and circular polarizations. (**b**) Confinement potential with and without the presence of a magnetic field. (**c**) Laser-dressed potential for the three values of laser parameter α_0.

The term V_d is the laser-dressed potential, and this is calculated as an average of the potential by means of the following integral:

$$V_d = \frac{e^2 B^2}{8} \int_0^{\frac{2\pi}{\omega}} \frac{(X^2(t) + Y^2(t))}{m_c^*} \, dt + \frac{\omega}{2\pi} \int_0^{\frac{2\pi}{\omega}} V(X(t), Y(t)) \, dt \,, \tag{7}$$

where $X(t) = x + c_x \alpha_0 \cos(\omega t)$, $Y(t) = y + c_y \alpha_0 \cos(\omega t + \pi/2)$, and

$$c_x = \begin{cases} 1 & \text{linear} \\ \frac{1}{\sqrt{2}} & \text{circular} \end{cases} \qquad c_y = \begin{cases} 0 & \text{linear} \\ \frac{1}{\sqrt{2}} & \text{circular} \end{cases}. \tag{8}$$

Here, the last coefficients were defined by convenience to tune the ILF-laser parameter intensity α_0 for the two polarizations, linear and circular, according to the definitions in Equation (8). Equation (7) is solved via numerical integration. The laser parameter α_0 is expressed in terms of the geometrical domains $\alpha_0^{in} = \frac{eA}{\sqrt{2}m_{in}^*\omega} \sim \frac{\sqrt{I_0}}{\omega^2}$ (I_0 is the laser intensity), and $\alpha_0^{out} = \alpha_0^{in} \frac{m_{in}^*}{m_{out}^*}$ are the inner (GaAs) and outer (AlGaAs) laser parameters of the DQR, respectively. For the laser dressing potential, see the Appendix A at the end.

The terms Rashba and Dresselhaus are obtained from the following two expressions

$$H_R = \alpha(\boldsymbol{\sigma} \times \mathbf{k})_z = \alpha(\sigma_x k_y - \sigma_y k_x), \qquad H_D = \beta(\sigma_x k_x - \sigma_y k_y) \tag{9}$$

When expanding these terms, each of the elements of the matrix H is obtained.

$$
\begin{aligned}
H_{11} &= H_0 + \frac{1}{2} g \mu_B B \\
H_{22} &= H_0 - \frac{1}{2} g \mu_B B \\
H_{12} &= (\alpha - i\beta)\frac{\partial}{\partial x} + (\beta - i\alpha)\frac{\partial}{\partial y} + \alpha \frac{eB}{2\hbar}(x - iy) - \beta \frac{eB}{2\hbar}(y - ix) \\
H_{21} &= -(\alpha + i\beta)\frac{\partial}{\partial x} - (\beta + i\alpha)\frac{\partial}{\partial y} + \alpha \frac{eB}{2\hbar}(x + iy) - \beta \frac{eB}{2\hbar}(y + ix)
\end{aligned}
\tag{10}
$$

In order to evaluate the optical response of the system, the following expression for the linear absorption coefficient was used:

$$\theta_{jl} = \omega \sqrt{\frac{\mu_0}{\varepsilon_0\,\varepsilon}} \frac{|M_{jl}|^2\, e^2\, \rho_{jl}\, \hbar\, \Gamma_{jl}}{(E_{jl} - \hbar\,\omega)^2 + (\hbar\,\Gamma_{jl})^2} \tag{11}$$

In this article, the expression for calculating the matrix elements is given by

$$M_{jl} = \iint \left[(\phi_\uparrow^*)_j\, \xi\, (\phi_\uparrow)_l + (\phi_\downarrow^*)_j\, \xi\, (\phi_\downarrow)_l \right] dx dy \tag{12}$$

These elements of the transition from state l to j were calculated for different types of polarization, linear ($\xi = x$), right circular $\left(\xi = \frac{x + i\,y}{\sqrt{2}} \right)$, and left circular $\left(\xi = \frac{x - i\,y}{\sqrt{2}} \right)$.

Finally, to solve for the uncoupled xy-motion of the electrons in the DQR, we used the finite element method, as implemented in the COMSOL Multiphysics software package [31–33].

3. Results and Discussion

The parameters used in this study are $\mu_0 = 1.257 \times 10^{-6}$ Tm/A, $m^*(GaAs) = 0.067\, m_0$, $m^*(Al_xGa_{1-x}As) = 0.093\, m_0$, $V(Al_xGa_{1-x}As) = 262$ meV, $\varepsilon = 12.58$, $\hbar\Gamma = 0.5$ meV, Landé factor $g = -2.15$, Rashba coefficient $\alpha = 5.4$ meV·nm, and Dresselhaus coefficient $\beta = 10.8$ meV·nm. Here, m_0 is the free electron mass.

Figure 1 shows a diagram of the GaAs-AlGaAs double quantum ring, with the profile taken from the work of Kuroda et al. [19] (in that study, the profile was obtained through AFM characterization measurements). An azimuthal symmetry was assumed, which allowed for a reduction in computational cost since the solution in the azimuthal angle co-ordinate is known analytically. Thus, the problem is reduced in numerical terms to the solution of a two-variable differential equation. A three-dimensional diagram of the double ring is shown in panel 1(a), where it can be seen that the variable height along the radial direction is small compared to the dimensions of the (x, y)-plane, which allows for obtaining adequate solutions by using the adiabatic approximation. In panel 1(a), the magnetic field vector (in the z-direction) is also shown, as well as two more vectors representing the polarization of the intense nonresonant laser, that is, in the x-direction (linear) and right circular. A cross-section of the confinement potential due to the variable height, without and with the presence of a magnetic field, B = 0 and 5 T, respectively, is presented in panel 1(b). It can be observed that the magnetic field generates significant changes in confinement in the outer ring. In panel 1(c), the laser-dressed potential for the two values of the laser parameter and in the absence of the fields for comparison purposes is reported. The value of alpha0 = 10 nm generates a lower barrier (approx. 190 meV) when compared to 262 meV without laser effects, and this also eliminates the double ring behavior of the geometry. For the higher laser field, a double ring appears with the appearance of a barrier in the area where, fundamentally, there is greater height for the first ring. These effects exhibited under the presence of the laser allow for treating the system as if it has another geometry (reference article).

The energies of a double GaAs-AlGaAs ring as a function of the magnetic field, both with and without SOI effects, are shown in Figure 2a and Figure 2b, respectively. In Figure 2a, the electron is confined in the outer ring, which is precisely the one that presents changes in its effective potential due to the magnetic field, as observed in Figure 1b, where the increase in potential generally leads to higher energy, with oscillations between states. In Figure 2b, with SOI activated, the states for spin up and down are differentiated. From Equation (2), it can be seen that the Zeeman term only appears in the presence of a magnetic field, unlike the SOI Rashba and Dresselhaus terms, which appear even without a magnetic field. This is evident in Figure 2b, where for B = 0, the first excited state of Figure 1b appears as two distinct states, even in the absence of a magnetic field. The inclusion of a magnetic field further accentuates the SOI effects; for example, the ground state is quasi-degenerate for very small magnetic fields (B <= 0.5). As the intensity of the field increases, the separation of the states becomes more pronounced, including the appearance

of oscillations between the ground state and the first excited state. The complexity of the spectrum under spin effects is not only due to the emergence of new states or breaking degeneracies; note that for Figure 2a, as the magnetic field increases, the ground state has a symmetry that comes from higher states in the absence of a field. In contrast, when spin is taken into account, the ground and first excited states are separated from the higher states, indicating that the symmetry for these two states does not become that of the higher energy states. This means that spin-orbit interaction not only causes changes in energy values but also exhibits important qualitative changes.
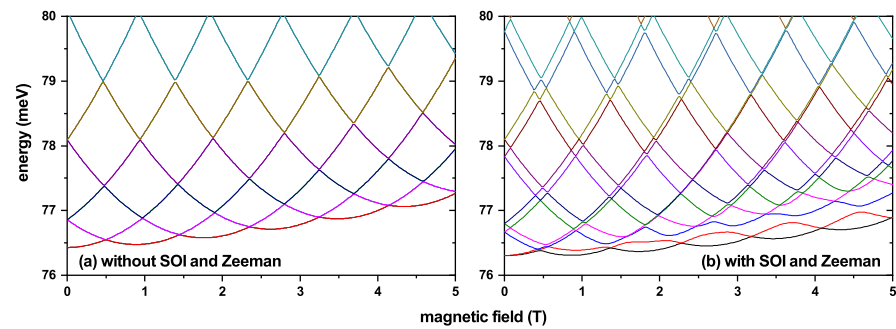
Figure 2. Electron energy in a double GaAs-Al$_{0.3}$Ga$_{0.7}$As quantum ring as a function of a magnetic field withtout (**a**) and with (**b**) SOI and Zeeman effects.

Figure 3 displays the energy as a function of the magnetic field in a double GaAs/AlGaAs ring, both without (first column) and with (second column) spin effects. Additionally, the presence of an intense nonresonant laser with linear polarization (x-direction) is shown for two laser parameter values: 10 nm (first row) and 20 nm (second row). Using an ILF with linear polarization destroys the cylindrical symmetry of the problem, which is most evident in the lowest states, where it is observed that, for instance, when the laser intensity is increased (Figure 3c,d), more states lose the characteristic oscillation that occurs in the absence of a laser. These changes in the energy spectra are equivalent to the changes in the geometry of the rings, but in this case, they result from the change in confinement created by the laser. Figure 3d shows that while spin effects differentiate the states as the field increases, a large value of the laser parameter inhibits the separation between the lowest energy states.

In Figure 4, energy is plotted as a function of the laser parameter, which is related to the intensity of the electromagnetic wave used. In addition, a magnetic field of 5 T was applied in the z-direction. In order to observe the changes induced by the spin in the spectrum, it is reported both in the absence (a) and under the effects of spin (b). The selected polarization increases the values of the barriers so that, as the laser parameter increases, confinement is induced for the lowest states along the y-axis. In Figure 4a, it can be seen that a higher laser intensity favors the separation of some states, which, in the absence of ILF, are quasi-degenerate. When spin interaction effects are included (Figure 4b), it becomes evident that for higher values of the laser parameter, the effect of ILF predominates over the state separation caused by spin. This is evident in the spectrum for the states that are separated in the absence of ILF and then come together when the laser parameter is increased.

Figure 5 displays the energy as a function of the magnetic field for a double GaAs/AlGaAs ring, both without (first column) and with (second column) spin effects. Additionally, the presence of an intense nonresonant laser with right circular polarization is shown for two values of the laser parameter: 10 nm (first row) and 20 nm (second row). These results highlight that the inclusion of ILF with circular polarization does not result in any loss of symmetry in the structure, unlike when linear polarization is included, which causes a loss of azimuthal symmetry. As such, the typical oscillations of the states as a function of the magnetic field observed in quantum rings are preserved with circular polarization. In accordance with the effective potential generated by the ILF, the energies are higher

when the laser parameter is increased, and a lower density of states per unit energy is also observed. This has important implications for potential applications since the intraband transition energies can be fine-tuned through the inclusion of ILF.
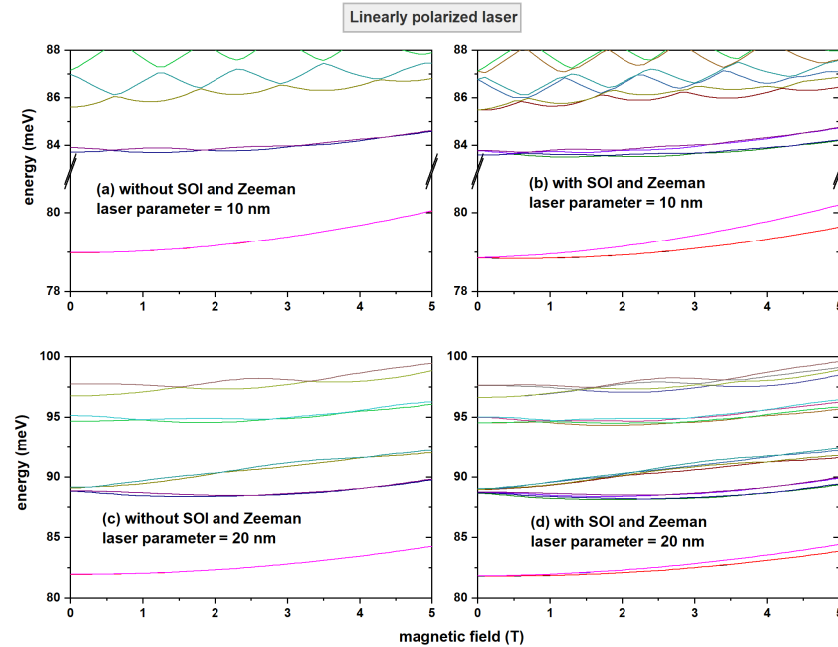
Figure 3. Electron energy in a double GaAs-Al$_{0.3}$Ga$_{0.7}$As quantum ring as a function of magnetic field and under the presence of a linearly x polarized intense laser field (ILF) for two laser parameter values: α_0: 10 nm and 20 nm.
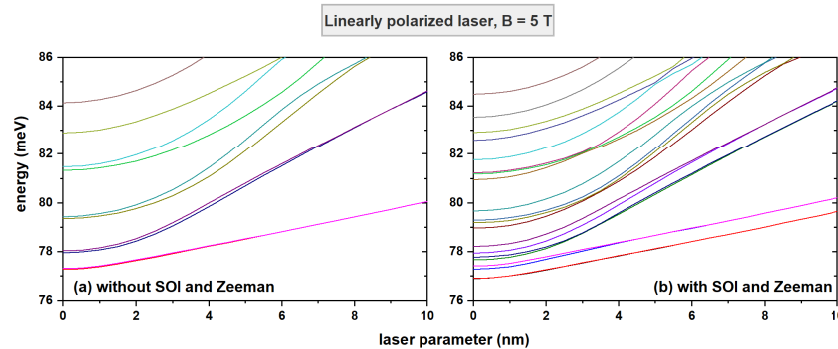
Figure 4. Comparative behavior of electron energy levels in a double GaAs-Al$_{0.3}$Ga$_{0.7}$As quantum ring as a function of the linearly polarized intense laser field parameter α_0 in the presence of a magnetic field and for two different cases: (**a**) without SOI and Zeeman and (**b**) with SOI and Zeeman.

In Figure 6, the squared matrix elements for transitions 1–2 and 1–3 are displayed as a function of the magnetic field in the first and second columns, respectively. The first row shows a calculation that incorporates both the SOI and the Zeeman effects, whereas the second row shows a calculation without the spin effect. In each of the four panels of Figure 6, we can observe the complementarity between right and left circular polarization since, in general, when one is activated, the other loses its magnitude. For the specific values of the magnetic field, there is even a drastic shift from one to the other. Note that in Figure 6a,b, the matrix elements either strengthen or weaken gradually, exhibiting behavior closer to what is expected for this phenomenon. The changes are only abrupt at specific values of the magnetic field; for example, in Figure 6a, at 4.1 T, there is an activation/deactivation of the transition depending on whether the polarization of the incident beam is right or left circular. In Figure 6c,d, when the contribution of spin is not included, the value of the matrix elements remains practically constant with the increase in the magnetic field,

only it is observed that the type of circular polarization activates the transition for different ranges of the field. In Figure 6b, we observe a loss of complementarity between the two polarizations used since transition 1–3 becomes only a part of the structure of a more complex spectrum with the appearance of more states due to spin interaction. These results allow us to highlight the importance of including spin effects in this type of work since the quantitative and qualitative changes are not negligible.
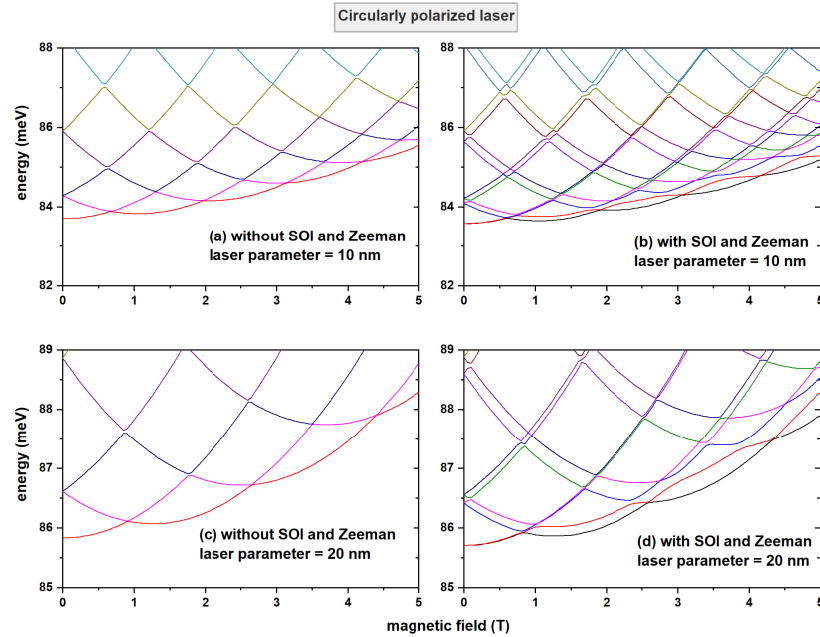
Figure 5. Electron energy in a double GaAs-Al$_{0.3}$Ga$_{0.7}$As quantum ring as a function of magnetic field and under the presence of a circularly polarized intense laser field (ILF) for two laser parameter values: α_0: 10 nm (first line) and 20 nm (second line).
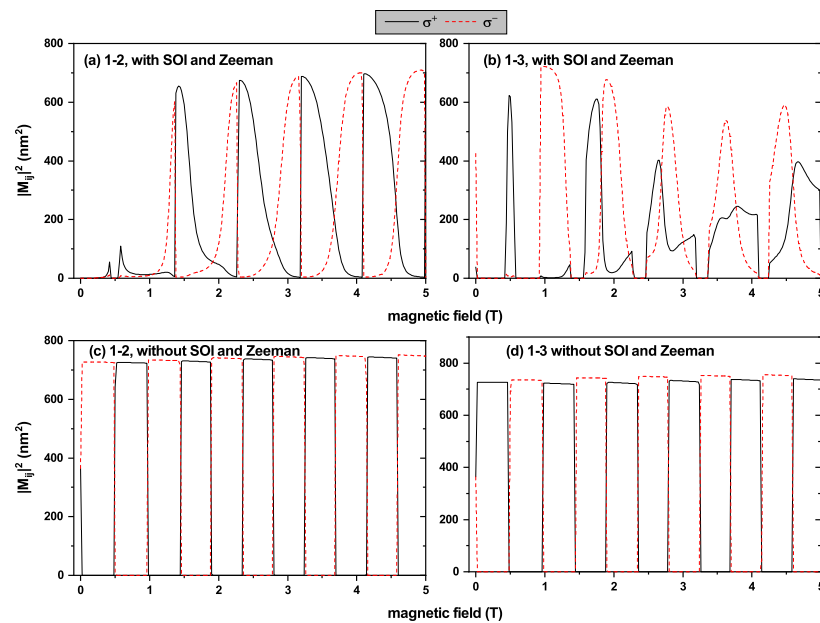
Figure 6. Squared matrix elements in a double GaAs-Al$_{0.3}$Ga$_{0.7}$As quantum ring as a function of magnetic field for right and left circularly polarized laser fields, σ^+ and σ^-, respectively. In panels (**a**,**b**), the SOI and Zeeman contributions are included; in contrast, for panels (**c**,**d**), the SOI and Zeeman contributions are turned off. For both conditions, the transitions 1–2 and 1–3 are studied.

Finally, in Figure 7, the results obtained for the linear absorption coefficient due to the 1–2 transition are reported without the inclusion of spin interaction (Figure 7a) and with the contribution of spin interaction (Figure 7b). Three values of the magnetic field were taken, which were applied in the z-direction, B = 0, 2.5, 5, T. The continuous lines represent right circular polarization, and the dashed lines represent left circular polarization. In Figure 7a, it is highlighted that in the absence of a magnetic field, the result is the same for any of the polarizations, no matter the kind of polarization. In contrast, when the SOI and Zeeman effects are included, in the absence of a magnetic field $B = 0$, the results are different depending on the polarization. Note that the absorption values are reduced when the effects of spin-orbit interaction are considered.
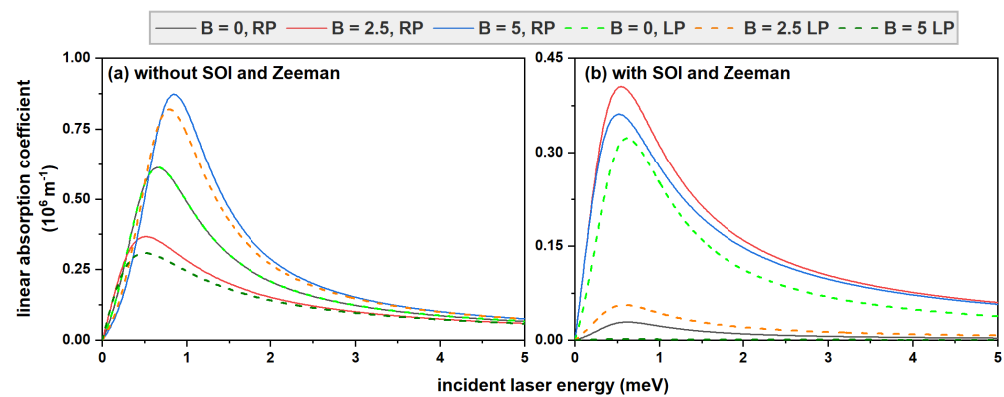
Figure 7. Linear absorption coefficient as a function of incident laser energy in a double GaAs-Al$_{0.3}$Ga$_{0.7}$As quantum ring for three values of the magnetic field: $B = 0$, 2.5, and 5 T. Panel (**a**) does not include the spin interactions, whereas in (**b**), it is added. The solid and dashed lines correspond to right and left circular laser polarizations, respectively.

4. Conclusions

We have investigated the behavior of electron energy levels in a double GaAs-AlGaAs quantum ring within the effective mass approximation through a realistic confining potential—which was taken from experimental reports—and dressed by the influence of an intense nonresonant laser field. The model also assumes the presence of an externally applied magnetic field and includes the effects of Zeeman and spin-orbit interaction. The latter is considered both in the Rashba and Dresselhaus formulations.

As expected, spin-orbit coupling causes a splitting of the degenerate levels, even at a zero magnetic field, but keeps the ground state oscillations, which actually disappear when an intense laser field acts upon the system. A linearly polarized laser field also removes some degeneracies, but in combination with spin-orbit interaction, the spectrum becomes completely resolved. The application of a circularly polarized laser field keeps the oscillatory variation of the ground state as a function of the magnetic field while raising up the whole spectrum by almost 10 meV.

Spin-orbit influence is responsible for a significant modification of the electric dipole moment off-diagonal matrix elements that are associated with transitions from the ground to the first two excited states. This is reflected in the linear optical absorption coefficient in the form of a noticeable reduction in resonant peak amplitude.

Author Contributions: M.E.M.-R., C.A.D. and A.L.M.: Conceptualization, formal analysis, writing; methodology, A.R. and J.A.V. software, methodology, formal analysis, investigation, writing, R.L.R., M.S., O.M., J.S.-O., G.E.E.-S., C.H. and D.A.D.: Formal analysis, investigation, supervision, writing. All authors have read and agreed to the published version of the manuscript.

Institutional Review Board Statement: Not applicable.

Informed Consent Statement: Not applicable.

Data Availability Statement: No new data were created or analyzed in this study. Data sharing is not applicable to this article.

Conflicts of Interest: The authors declare no conflict of interest.

Appendix A

Without the presence of the magnetic field, spin-orbit interaction, and Zeeman effect; the single-electron under a nonresonant high-frequency laser field is a simplified case. In this appendix, the linear polarization case from Equation (3), $\kappa = 0$, is inspected.

Let us analyze the interaction between a confined carrier and a laser beam considered as an ideal monochromatic plane wave, as described by the magnetic vector potential $\mathbf{A}_l(\mathbf{r}, t) = \mathbf{A}_0 \exp[i(\mathbf{k} \cdot \mathbf{r} - \omega t)]$, with $\mathbf{r}$ being the position vector. The laser field is taken from a semiclassical point of view, and for convenience, the Coulomb gauge is used. This means that the conditions $\nabla \cdot \mathbf{A}(\mathbf{r}, t) = 0$ (vector potential) and $\phi = 0$ (scalar potential) are met. The temporal Schrödinger equation under these conditions is given by

$$i\hbar \frac{\partial}{\partial t} \psi_L(\mathbf{r}, t) = \left[\frac{1}{2m^*} (\hat{p} - e\mathbf{A}(\mathbf{r}, t))^2 + V(\mathbf{r}) \right] \psi_L(\mathbf{r}, t), \tag{A1}$$

where the subscript in Ψ_L indicates that the equation is in the so-called laboratory (stationary) frame.

By expanding the first term of the Hamiltonian, the product $\hat{p} \cdot \mathbf{A}(\mathbf{r}, t)$ commutes due to the Coulomb gauge. We may further refer to the "size" of the system as being the span of the domain where potential $V(\mathbf{r})$ has a significant variation (the domain of interest). We assume that the wavelength of the laser field is much larger than the size of the system, and the dependence on $\mathbf{r}$ of $\mathbf{A}$ can be neglected; thus, only the temporal dependency will be kept. In mathematical language, $\mathbf{A}(\mathbf{r}, t) = \mathbf{A}(t)e^{i\mathbf{k} \cdot \mathbf{r}} = \mathbf{A}(t)(1 + i\mathbf{k} \cdot \mathbf{r} + \cdots) \approx \mathbf{A}(t)$, which is the well-known dipole approximation. By using the momentum operator representation in co-ordinates $\hat{p} = -i\hbar\nabla$, the Schrödinger equation can be rewritten as

$$i\hbar \frac{\partial}{\partial t} \psi_L(\mathbf{r}, t) = \left[-\frac{\hbar^2}{2m^*} \nabla^2 + \frac{i\hbar e}{m^*} \mathbf{A}(t) \cdot \nabla + \frac{e^2}{2m^*} \mathbf{A}^2(t) + V(\mathbf{r}) \right] \psi_L(\mathbf{r}, t). \tag{A2}$$

This equation can be simplified using the Kramers-Henneberger transformation [34,35]. The idea under this technique of including the laser field effect is transferring the time dependence from the kinetic to potential term [36], which is why this transformation is largely known as the laser-dressing of the potential. It can be subdivided into two transformations: U_1 and U_2 [37]. In the first, the $\mathbf{A}^2(t)$ term is reduced, and in the second, the $\mathbf{A}(t)$ term is eliminated.

The transformation U_1 is an operator defined as

$$U_1 = e^{-\frac{ie^2}{2m^*\hbar} \int^t \mathbf{A}^2(t')dt'}, \tag{A3}$$

and the new, unknown wave function in the velocity frame will be

$$\psi_v(\mathbf{r}, t) = U_1^\dagger \psi_L(\mathbf{r}, t). \tag{A4}$$

By applying the $U_1^\dagger$ transformation in Equation (A2), one will obtain

$$i\hbar U_1^\dagger \frac{\partial}{\partial t}[U_1 \psi_v(\mathbf{r}, t)] =$$
$$U_1^\dagger \left[-\frac{\hbar^2}{2m^*}\nabla^2 + \frac{i\hbar e}{m^*}\mathbf{A}(t)\cdot\nabla + \frac{e^2}{2m^*}\mathbf{A}^2(t) + V(\mathbf{r}) \right] U_1 \psi_v(\mathbf{r}, t). \tag{A5}$$

Because U_1 is independent of $\mathbf{r}$, on the right side of the equation, only the terms of $\mathbf{A}^2$ and $\mathbf{A}(t)$ vary when this operator is applied.

By expanding the derivative on the left side of the previous equation, we obtain

$$U_1^\dagger \frac{e^2}{2m^*}\mathbf{A}^2(t)U_1 \psi_v(\mathbf{r}, t) + i\hbar\frac{\partial}{\partial t}\psi_v(\mathbf{r}, t) =$$
$$U_1^\dagger \left[-\frac{\hbar^2}{2m^*}\nabla^2 + \frac{i\hbar e}{m^*}\mathbf{A}(t)\cdot\nabla + \frac{e^2}{2m^*}\mathbf{A}^2(t) + V(\mathbf{r}) \right] U_1 \psi_v(\mathbf{r}, t). \tag{A6}$$

Note that the term $\mathbf{A}^2(t)$ is eliminated since it appears on the two sides of the equation. In this new frame, the resulting equation is

$$i\hbar\frac{\partial}{\partial t}\psi_v(\mathbf{r}, t) = \left[-\frac{\hbar^2}{2m^*}\nabla^2 + \frac{i\hbar e}{m^*}\mathbf{A}(t)\cdot\nabla + V(\mathbf{r}) \right] \psi_v(\mathbf{r}, t). \tag{A7}$$

The second part aims to eliminate the term associated with $\mathbf{A}\cdot\nabla$. For this, we use the following transformation:

$$U_2 = e^{-\frac{i}{\hbar}\boldsymbol{\alpha}(t)\cdot\widehat{p}} \text{ with } \boldsymbol{\alpha}(t) = -\frac{e}{m^*}\int^t \mathbf{A}(t')dt'. \tag{A8}$$

Note that U_2 can be rewritten as $U_2 = e^{\frac{e}{m^*}\int^t \mathbf{A}(t')dt'\cdot\nabla}$, the new wavefunction will be $\psi_{KH}(\mathbf{r}, t) = U_2^\dagger \psi_v(\mathbf{r}, t)$, and by applying this transformation to Equation (A7), one may obtain

$$i\hbar U_2^\dagger \frac{\partial}{\partial t}[U_2 \psi_{KH}(\mathbf{r}, t)] =$$
$$U_2^\dagger \left[-\frac{\hbar^2}{2m^*}\nabla^2 + \frac{i\hbar e}{m^*}\mathbf{A}(t)\cdot\nabla + V(\mathbf{r}) \right] U_2 \psi_{KH}(\mathbf{r}, t). \tag{A9}$$

Expanding the time derivative on the left side of the equation will lead to

$$U_2^\dagger \left[\frac{i\hbar e}{m^*}\mathbf{A}(t)\cdot\nabla \right] U_2 \psi_{KH}(\mathbf{r}, t) + i\hbar\frac{\partial}{\partial t}\psi_{KH}(\mathbf{r}, t) =$$
$$U_2^\dagger \left[-\frac{\hbar^2}{2m^*}\nabla^2 + \frac{i\hbar e}{m^*}\mathbf{A}(t)\cdot\nabla + V(\mathbf{r}) \right] U_2 \Psi_{KH}(\mathbf{r}, t). \tag{A10}$$

The term $\frac{i\hbar e}{m^*}\mathbf{A}\cdot\nabla$ is eliminated since it appears on both sides of the equation. Hence, the simplified equation is given by

$$i\hbar\frac{\partial}{\partial t}\psi_{KH}(\mathbf{r}, t) = U_2^\dagger \left[-\frac{\hbar^2}{2m^*}\nabla^2 + V(\mathbf{r}) \right] U_2 \psi_{KH}(\mathbf{r}, t). \tag{A11}$$

The transformation leaves invariant the momentum operator. Therefore, we only concentrate on showing explicitly the effect of the transformation on the term $V(\mathbf{r})$. For this development, we use the Campbell-Baker-Hausdorff identity $e^{\widehat{A}}\widehat{B}e^{-\widehat{A}} = \widehat{B} + [\widehat{A}, \widehat{B}] + [\widehat{A}, [\widehat{A}, \widehat{B}]]/2! + \cdots$, and we get

$$
\begin{aligned}
U_2^{\dagger} V(\mathbf{r}) U_2 &= e^{\frac{i}{\hbar}\boldsymbol{\alpha}(t)\cdot\widehat{p}} V(\mathbf{r}) e^{-\frac{i}{\hbar}\boldsymbol{\alpha}(t)\cdot\widehat{p}} \\
&= V(\mathbf{r}) + [\boldsymbol{\alpha}(t) \cdot \nabla] V(\mathbf{r}) + \frac{1}{2!}[\boldsymbol{\alpha}(t) \cdot \nabla]^2 V(\mathbf{r}) + \cdots \\
&= V[\mathbf{r} + \boldsymbol{\alpha}(t)].
\end{aligned}
\tag{A12}
$$

This means that the only time dependence of the equation in the Kramers-Henneberger frame is through the potential V. Note that the U_2 operator generates a translation given by $\boldsymbol{\alpha}(t)$. As a result, we have an effective potential that accounts for the interaction laser system, commonly called laser-dressed potential. This indicates that the shape of the new potential is a direct consequence of the laser effect. Therefore, the Schrödinger equation in this KH-frame has the form

$$
i\hbar\frac{\partial}{\partial t}\psi_{KH}(\mathbf{r},t) = \left[-\frac{\hbar^2}{2m^*}\nabla^2 + V[\mathbf{r} + \boldsymbol{\alpha}(t)]\right]\psi_{KH}(\mathbf{r},t).
\tag{A13}
$$

An additional issue can be highlighted with respect to $\boldsymbol{\alpha}(t)$: by calculating the second derivative with respect to the time of $\boldsymbol{\alpha}(t)$, we have $\ddot{\boldsymbol{\alpha}}(t) = \frac{e}{m^*}\mathbf{E}(t)$, where $\mathbf{E}(t)$ is the electric field. Hence, $\boldsymbol{\alpha}(t)$ is interpreted as the classical displacement of the electron under the electric field $\mathbf{E}(t)$ associated with the laser wave. In the case of a steady laser field, i.e., $\mathbf{E}(t) = E_0\sin(\omega t)\,\mathbf{x}$, one may observe that $\boldsymbol{\alpha}(t) = \frac{eE_0}{m^*\omega^2}\sin(\omega t)\,\mathbf{x}$. This can be rewritten as $\boldsymbol{\alpha}(t) = \alpha_0\sin(\omega t)\,\mathbf{x}$, where $\alpha_0 = \frac{eE_0}{m^*\omega^2}$ represents the oscillation amplitude of the electron under the laser field (called the laser-dressing parameter). E_0 is the amplitude of the electric field, and ω is the angular frequency of the laser.

The Floquet theory provides a solution for the Equation (A13) [35,38]:

$$
\psi_{KH}(\mathbf{r},t) = e^{-\frac{E_{KH}}{\hbar}t}\sum_{n}\psi_n^{KH}(\mathbf{r})e^{-in\omega t},
\tag{A14}
$$

where E_{KH} is the quasi-energy of Floquet. Additionally, the potential V can be expanded by the Fourier series as

$$
V[\mathbf{r} + \boldsymbol{\alpha}(t)] = \sum_{m=-\infty}^{\infty} V_m(\alpha_0;\mathbf{r})e^{-im\omega t},
\tag{A15}
$$

with

$$
V_m(\alpha_0;\mathbf{r}) = \frac{i^m}{\pi}\int_{-1}^{1} V(\mathbf{r} + \alpha_0 u\,\mathbf{x})T_m(u)(1-u^2)^{-1/2}du,
\tag{A16}
$$

where $T_m(u)$ are the Chebyshev polynomials. When taking into account the fact that we use laser fields with high frequency (when compared to the characteristic interlevel transition frequencies of the system), it is enough to consider the lowest order in Equation (A16):

$$
V_0(\alpha_0,\mathbf{r}) = \frac{1}{\pi}\int_{-1}^{1}\frac{V(\mathbf{r} + \alpha_0 u\mathbf{x})}{\sqrt{1-u^2}}du.
\tag{A17}
$$

By making a trigonometric substitution, the laser-dressed potential can be written as

$$
V_0(\alpha_0,\mathbf{r}) = \frac{\omega}{2\pi}\int_{0}^{2\pi/\omega} V(\mathbf{r} + \alpha_0\sin(\omega t)\,\mathbf{x})dt.
\tag{A18}
$$

Finally, the Schrödinger equation will have the atemporal form:

$$\left[-\frac{\hbar^2}{2m^*}\nabla^2 + V_0(\alpha_0, \mathbf{r}) \right] \Psi(\mathbf{r}) = E\Psi(\mathbf{r}). \tag{A19}$$

Note that this equation only depends on $\mathbf{r}$ since $V_0(\alpha_0, \mathbf{r})$ corresponds to the average of the oscillating potential function:

$$V_0(\alpha_0, \mathbf{r}) = \frac{1}{T}\int_0^T V(\mathbf{r} + \boldsymbol{\alpha}(t))dt. \tag{A20}$$

References

1. Abbarchi, M.; Mastrandrea, C.A.; Vinattieri, A.; Sanguinetti, S.; Mano, T.; Kuroda, T.; Koguchi, N.; Sakoda, K.; Gurioli, M. Photon Antibunching in Double Quantum Ring Structures. *Phys. Rev. B* **2009**, *79*, 085308. [CrossRef]
2. Gallardo, E.; Martínez, L.J.; Nowak, A.K.; Sarkar, D.; Sanvitto, D.; van der Meulen, H.P.; Calleja, J.M.; Prieto, I.; Granados, D.; Taboada, A.G.; et al. Single-Photon Emission by Semiconductor Quantum Rings in a Photonic Crystal. *J. Opt. Soc. Am. B* **2010**, *27*, A21–A24. [CrossRef]
3. Sanguinetti, S.; Koguchi, N.; Mano, T.; Kuroda, T. Droplet Epitaxy Quantum Ring Structures. *J. Nanoelectron. Optoelectron.* **2011**, *6*, 34–50. [CrossRef]
4. Wang, D.; Zhu, T.; Oliver, R.A.; Hu, E.L. Ultra-low-threshold InGaN/GaN Quantum Dot Micro-Ring Lasers. *Opt. Lett.* **2018**, *43*, 799–802. [CrossRef]
5. Mandel, A.M.; Oshurko, V.B.; Pershin, S.M.; Karpova, E.E.; Artemova, D.G. Tunable-Frequency Lasing on Thin Semiconductor Quantum Rings. *Dokl. Phys.* **2021**, *66*, 160–163. [CrossRef]
6. Wu, J.; Li, Z.; Shao, D.; Manasreh, M.O.; Kunets, V.P.; Wang, Z.M.; Salamo, G.J.; Weaver, B.D. Multicolor Photodetector Based on GaAs Quantum Rings Grown by Droplet Epitaxy. *Appl. Phys. Lett.* **2009**, *94*, 171102. [CrossRef]
7. Samadzadeh, R.; Zavvari, M.; Hosseini, R. Tunable Far Infrared Detection Using Quantum Rings-in-Well Intersubband Photodetectors. *Opt. Quant. Electron.* **2015**, *47*, 3555–3565. [CrossRef]
8. Wu, J.; Wang, Z.; Dorogan, V.; Lee, J.; Mazur, Y.; Kim, E.S.; Salamo, G. Effects of Rapid Thermal Annealing on the Optical Properties of Strain-Free Quantum Ring Solar Cells. *Nanoscale Res. Lett.* **2013**, *8*, 5. [CrossRef]
9. Fujita, H.; James, J.; Carrington, P.J.; Marshall, A.R.J.; Krier, A.; Wagener, M.C.; Botha, J.R. Semiconductor Science and Technology. *Semicond. Sci. Technol.* **2014**, *29*, 035014. [CrossRef]
10. Baxevanis, B.; Pfannkuche, D. Spin Transitions in Semiconductor Quantum Rings. *J. Phys. Conf. Ser.* **2010**, *245*, 012023. [CrossRef]
11. Zipper, E.; Kurpas, M.; Sadowski, J.; Maska, M. Semiconductor Quantum Ring as a Solid-State Spin Qubit. *J. Phys. Condens. Matter* **2011**, *23*, 115302. [CrossRef]
12. Nagasawa, F.; Frustaglia, D.; Saarikoski, H.; Richter, K.; Nitta, J. Control of the Spin Geometric Phase in Semiconductor Quantum Rings. *Nat. Commun.* **2013**, *4*, 2526. [CrossRef]
13. Zamani, A.; Azargoshasb, T.; Niknam, E. Second and Third Harmonic Generations of a Quantum Ring with Rashba and Dresselhaus Spin-Orbit Couplings: Temperature and Zeeman Effects. *Phys. B* **2017**, *523*, 85. [CrossRef]
14. Pourmand, S.E.; Rezaei, G. The Rashba and Dresselhaus Spin-Orbit Interactions Effects on the Optical Properties of a Quantum Ring. *Phys. B* **2018**, *543*, 27. [CrossRef]
15. Pourmand, S.E.; Rezaei, G.; Vaseghi, B. Impacts of External Fields and Rashba and Dresselhaus Spin-Orbit Interactions on the Optical Rectification, Second and Third Harmonic Generations of a Quantum Ring. *Eur. Phys. J. B* **2019**, *92*, 96. [CrossRef]
16. Sigurdsson, H.; Kibis, O.V.; Shelykh, I.A. Optically induced Aharonov-Bohm effect in mesoscopic rings. *Phys. Rev. B* **2014**, *90*, 235413. [CrossRef]
17. Kozin, V.K.; Iorsh, I.V.; Kibis, O.V.; Shelykh, I.A. Quantum ring with the Rashba spin-orbit interaction in the regime of strong light-matter coupling. *Phys. Rev. B* **2018**, *97*, 155434. [CrossRef]
18. Kozin, V.K.; Iorsh, I.V.; Kibis, O.V.; Shelykh, I.A. Periodic array of quantum rings strongly coupled to circularly polarized light as a topological insulator. *Phys. Rev. B 2018*, *97*, 035416. [CrossRef]
19. Mano, T.; Kuroda, T.; Sanguinetti, S.; Ochiai, T.; Tateno, T.; Kim, J.; Noda, T.; Kawabe, M.; Sakoda, K.; Kido, G.; et al. Self-Assembly of Concentric Quantum Double Rings. *Nano Lett.* **2005**, *5*, 425. [CrossRef]
20. Kuroda, T.; Mano, T.; Ochiai, T.; Sanguinetti, S.; Noda, T.; Kuroda, K.; Sakoda, K.; Kido, G.; Koguchi, N. Excitonic Transitions in Semiconductor Concentric Quantum Double Rings. *Phys. E* **2006**, *32*, 46. [CrossRef]
21. Mühle, A.; Wegscheider, W.; Haug, R.J. Coulomb-Coupled Concentric Quantum Rings. *Phys. E* **2008**, *40*, 1246. [CrossRef]
22. Kim, J.S. Investigation of Various Optical Transitions in GaAs/$Al_{0.3}Ga_{0.7}$As Double Quantum Ring Grown by Droplet Epitaxy. *Phys. Status Solidi RRL* **2016**, *10*, 1862. [CrossRef]
23. Li, S.-S.; Xia, J.-B. Electronic Structures of GaAs/AlxGa1-xAs Quantum Double Rings. *Nanoscale Res. Lett.* **2006**, *1*, 167. [CrossRef]
24. Planelles, J.; Climente, J. Semiconductor Concentric Double Rings in a Magnetic Field. *Eur. Phys. J. B* **2005**, *48*, 65. [CrossRef]

25. Bejan, D.; Niculescu, E.C. Electronic and Optical Properties of Asymmetric GaAs Double Quantum Dots in Intense Laser Fields. *Phil. Mag.* **2016**, *96*, 1131–1149. [CrossRef]
26. Baghramyan, H.M.; Barseghyan, M.G.; Kirakosyan, A.A.; Ojeda, J.H.; Bragard, J.; Laroze, D. Modeling of Anisotropic Properties of Double Quantum Rings by the Terahertz Laser Field. *Sci. Rep.* **2018**, *8*, 6145. [CrossRef]
27. Barseghyan, M.G.; Mughnetsyan, V.N.; Baghramyan, H.M.; Ungan, F.; Pérez, L.M.; Laroze, D. Control of Electronic and Optical Properties of a Laser Dressed Double Quantum Dot Molecule by Lateral Electric Field. *Phys. E* **2021**, *126*, 114362. [CrossRef]
28. Khajeh Salehani, H. Optical Absorption in Concentric Double Quantum Rings. *Opt. Quantum Electron.* **2023**, *55*, 644. [CrossRef]
29. Vinasco, J.A.; Radu, A.; Tiutiunnyk, A.; Restrepo, R.L.; Laroze, D.; Feddi, E.; Mora-Ramos, M.E.; Morales, A.L.; Duque, C.A. Revisiting the adiabatic approximation for bound states calculation in axisymemetric and asymmetrical quantum structures. *Superlattices Micros* **2020**, *138*, 106384. [CrossRef]
30. Breuer, H.P.; Dietz, K.; Holthaus, M. A Remark on the Kramers-Henneberger Transformation. *Phys. Lett. A* **1992**, *165*, 341–346. [CrossRef]
31. COMSOL. *Multiphysics*; v. 5.4; COMSOL AB: Stockholm, Sweden, 2012.
32. COMSOL. *Multiphysics Reference Guide*; COMSOL: Stockholm, Sweden, 2012.
33. COMSOL. *Multiphysics Users Guide*; COMSOL: Stockholm, Sweden, 2012.
34. Henneberger, W.C. Perturbation method for atoms in intense light beams. *Phys. Rev. Lett.* **1968**, *21*, 12. [CrossRef]
35. Burnett, K.; Reed, V.C.; Knight, P.L. Atoms in ultra-intense laser fields. J. *Phys. B At. Mol. Opt.* **1993**, *26*, 561. [CrossRef]
36. Lima, F.M.S.; Amato, M.A.; Nunes, O.A.C.; Fonseca, A.L.A.; Enders, B.G.; da Silva, E.F., Jr. Unexpected transition from single to double quantum well potential induced by intense laser fields in a semiconductor quantum well. *J. Appl. Phys.* **2009**, *105*, 123111. [CrossRef]
37. Falaye, B.J.; Sun, G.-H.; Adepoju, A.G.; Liman, M.S.; Oyewumi, K.J.; Dong, S.-H. An electron of helium atom under a high-intensity lasr field. *Laser Phys.* **2017**, *27*, 026004. [CrossRef]
38. Gavrila, M. Atomic stabilization in superintense laser fields. *J. Phys. B At. Mol. Opt.* **2002**, *35*, R147–R193. [CrossRef]